**Supplementary information**

# Synergistic interface design of $Al_2O_3$-coated NMC811 and graphitic-based pre-lithiated anodes for enhanced full-cell performance

Ebru Doğan,[a] Rawdah Whba[a,b,*], Iqra Moeez[c], Kyung Yoon Chung[c], Ece Unur Yilmaz[d], Emine Altin[e], Mehmet Nurullah Ates[f,g], Serdar Altın [a,*]

[a]*Physics Department, Inonu University, Battalgazi, Malatya 44280, Türkiye*
[b]*Department of Chemistry, Faculty of Applied Sciences, Taiz University, 6803 Taiz, Yemen*
[c]*Energy Storage Research Center, Korea Institute of Science and Technology, Seoul 02792, Republic of Korea*
[d]*Bursa Teknik University, Department of Chemistry, 16310,Yıldırım, Bursa, Türkiye*
[e]*Vocational School of Health Service, Inonu University, Battalgazi, Malatya 44280, Türkiye*
[f]*Chemistry Department, Bogazici University, Bebek, İstanbul, Türkiye*
[g]*TÜBİTAK Rail Transport Technologies Institute, Energy Storage Division, TÜBİTAK Gebze Campus, 41470 Gebze, Kocaeli, Türkiye*

[*]Corresponding author at Physics Department, Inonu University, Malatya, Türkiye
*E-mail addresses: rawdahwhba@taiz.edu.ye* (R. Whba) & *serdar.altin@inonu.edu.tr* (S. Altin)

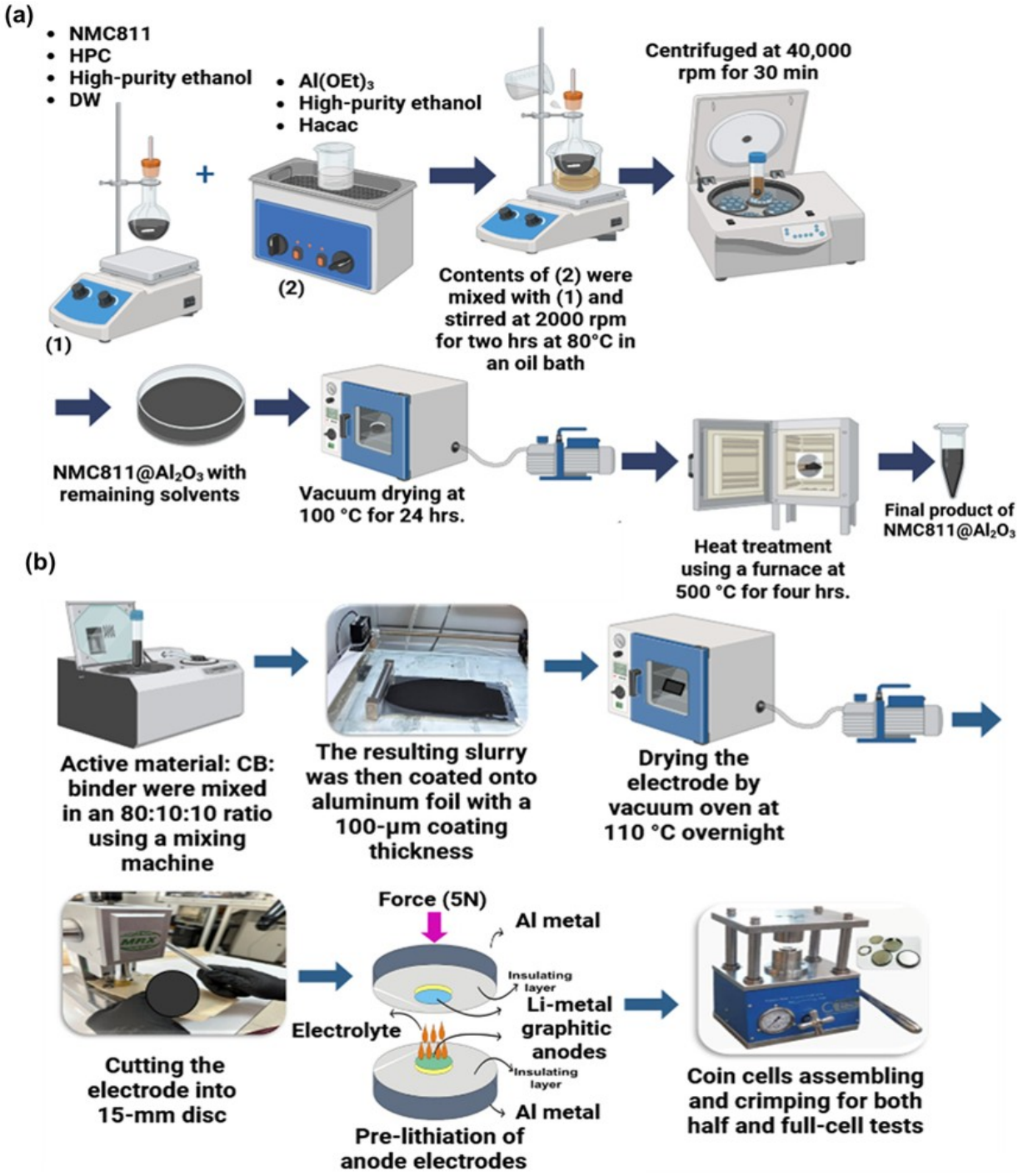


**Fig. S1** Schematic illustration of the process from $Al_2O_3$-coated NMC811 synthesis to full-cell performance testing. (a) Synthesis of NMC811@$Al_2O_3$ with varying coating ratios and (b) Preparation of cathode and anode electrodes, including anode pre-lithiation, followed by coin cell assembly for half-cell and full-cell electrochemical testing.

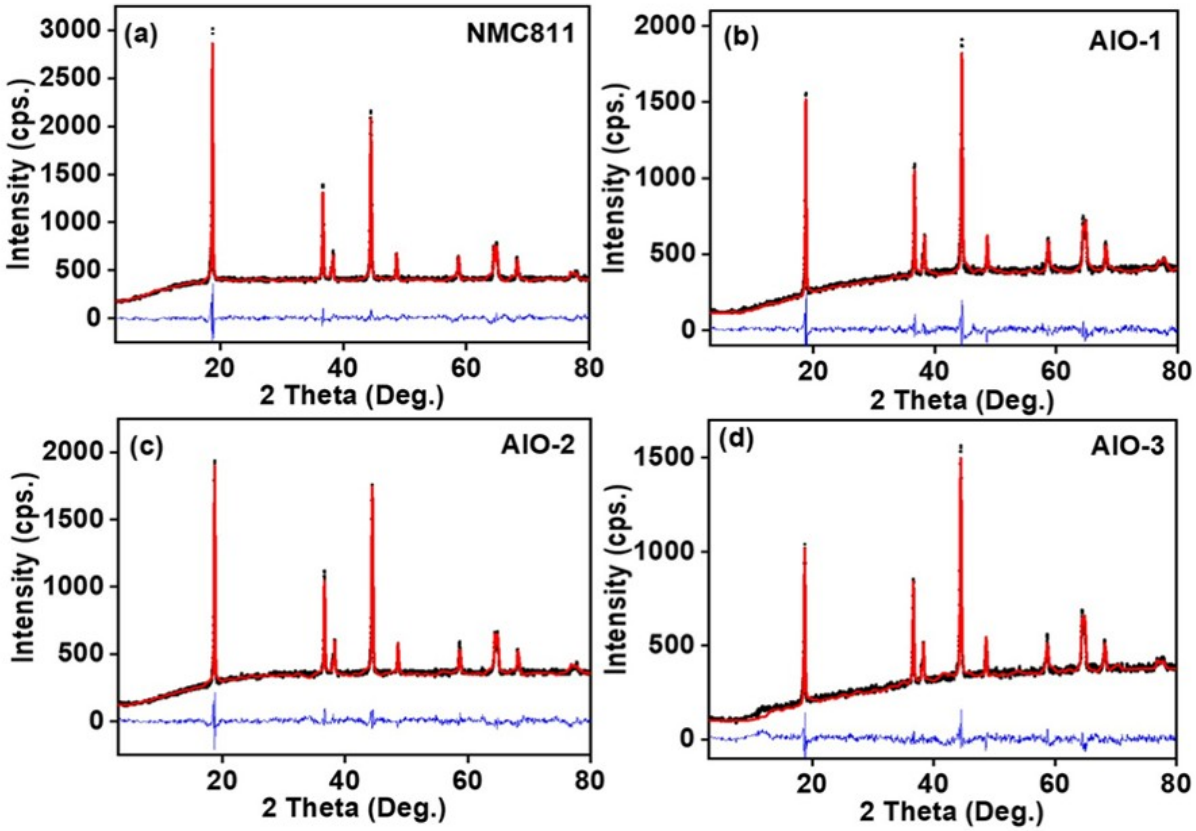


**Fig. S2** (a-d) XRD patterns of NMC811 and $Al_2O_3$-coated NMC811 powders.

**Table S1.** Rietveld Refinement results of NMC811 and $Al_2O_3$-coated NMC811 powders.

| Sample ID | Symmetry | *a* (Å) | *c* (Å) | Volume (Å$^3$) | $I_{(003)}/I_{(104)}$ | Bragg R-factor | Chi$^2$ |
|---|---|---|---|---|---|---|---|
| NMC811 | $R\bar{3}m$ | 2.8703(1) | 14.1927(3) | 101.26(4) | 1.49 | 7.6 | 1.3 |
| AlO-1 | $R\bar{3}m$ | 2.8752(1) | 14.2052(2) | 101.69(2) | 0.85 | 9.7 | 1.2 |
| AlO-2 | $R\bar{3}m$ | 2.8744(2) | 14.2015(2) | 101.62(3) | 1.13 | 7.9 | 1 |
| AlO-3 | $R\bar{3}m$ | 2.8728 (2) | 14.1940(2) | 101.45(3) | 0.69 | 10.3 | 0.8 |

**Table S2.** XRD peak positions at 2$\theta$ corresponding to the various crystallographic planes (*hkl*), along with the calculated crystallite sizes of NMC811 and $Al_2O_3$-coated NMC811 powders.

| NMC811 | | | AlO-1 | | | AlO-2 | | | AlO-3 | | |
|---|---|---|---|---|---|---|---|---|---|---|---|
| **2$\theta$** | **(*h k l*)** | **Crystallite size (nm)** | **2$\theta$** | **(*h k l*)** | **Crystallite size (nm)** | **2$\theta$** | **(*h k l*)** | **Crystallite size (nm)** | **2$\theta$** | **(*h k l*)** | **Crystallite size (nm)** |
| 18.681 | ( 0 0 3) | 46.6 | 18.699 | ( 0 0 3) | 48 | 18.679 | ( 0 0 3) | 46.3 | 18.7 | ( 0 0 3) | 39.1 |
| 36.62 | ( 1 0 1) | 45.8 | 36.58 | ( 1 0 1) | 40.9 | 36.561 | ( 1 0 1) | 42.5 | 36.6 | ( 1 0 1) | 38.4 |
| 37.96 | ( 0 0 6) | 17.3 | 37.96 | ( 0 0 6) | 13.3 | 37.961 | ( 0 0 6) | 20.4 | 38.021 | ( 0 0 6) | 11.6 |
| 38.28 | ( 0 1 2) | 29.1 | 38.259 | ( 0 1 2) | 27.1 | 38.221 | ( 0 1 2) | 27.3 | 38.261 | ( 0 1 2) | 25.9 |
| 44.401 | ( 1 0 4) | 38.2 | 44.38 | ( 1 0 4) | 35.7 | 44.36 | ( 1 0 4) | 36 | 44.4 | ( 1 0 4) | 34.5 |
| 48.6 | ( 0 1 5) | 38.3 | 48.58 | ( 0 1 5) | 27.8 | 48.541 | ( 0 1 5) | 33.4 | 48.6 | ( 0 1 5) | 31 |
| 58.64 | ( 1 0 7) | 23 | 58.64 | ( 1 0 7) | 25 | 58.621 | ( 1 0 7) | 32.9 | 58.68 | ( 1 0 7) | 28.2 |
| 64.401 | ( 0 1 8) | 21.5 | 64.381 | ( 0 1 8) | 17.1 | 64.38 | ( 0 1 8) | 16.2 | 64.421 | ( 0 1 8) | 18.7 |
| 68.16 | ( 1 1 3) | 27.2 | 64.819 | ( 1 1 3) | 15.1 | 64.78 | ( 1 1 3) | 16.8 | 64.819 | ( 1 1 3) | 15.5 |
| 77.682 | ( 1 1 6) | 14.4 | 68.12 | ( 1 1 6) | 27.7 | 68.08 | ( 1 1 6) | 30 | 68.158 | ( 1 1 6) | 24.9 |

**Table S3.** FTIR's wavenumber assignments of uncoated and $Al_2O_3$-coated NMC811 powders.

| FTIR assignment | Wavenumber ($cm^{-1}$) Sample ID | | | |
|---|---|---|---|---|
| | **NMC811** | **NMC811@ AlO-1** | **NMC811@ AlO-2** | **NMC811@ AlO-3** |
| Ni–O | 434 | 427 | 442 | 434 |
| Co–O | 551 | 548 | 543 | 536 |
| Mn–O | 657 | 657 | 704 | 694 |
| C–O stretching in $CO_3^{-2}$ | 868 & 1382 | 868 & 1384 | 864 & 1384 | 871 & 1384 |
| H–O–H bending | 1596 & 1640 | 1596 & 1651 | 1596 & 1648 | 1596 & 1640 |
| Al–O | NA | 1048 | 1048 | 1048 |

* NA is not available

**Table S4.** Raman spectra of $Al_2O_3$-coated NMC811 powders, highlighting characteristic vibrational modes associated with the $Al_2O_3$ layer.

| Sample ID | Raman Shift | Vibration mode | % Contribution |
|---|---|---|---|
| NMC811 | 406.6 | $E_g$ (Ni) | 11.3 |
| | 467.7 | $E_g$ (Co) | 17.6 |
| | 507.9 | $E_g$ (Mn) | 17.6 |
| | 552.4 | $A_{1g}$ (Ni) | 35.0 |
| | 586 | $A_{1g}$ (Co) | 11.8 |
| | 622.2 | $A_{1g}$ (Mn) | 6.7 |
| | 389 | $E_g$ (Ni) | 11.9 |
| | 451.5 | $E_g$ (Co) | 20.3 |
| | 506.7 | $E_g$ (Mn) | 32.0 |
| AlO-1 | 550.8 | $A_{1g}$ (Ni) | 24.6 |
| | 587.5 | $A_{1g}$ (Co) | 7.2 |
| | 623.7 | $A_{1g}$ (Mn) | 4.0 |
| | 389 | $E_g$ (Ni) | 6.7 |
| | 451.5 | $E_g$ (Co) | 15.3 |
| | 505.2 | $E_g$ (Mn) | 29.5 |
| AlO-2 | 548.5 | $A_{1g}$ (Ni) | 27.9 |
| | 586 | $A_{1g}$ (Co) | 11.7 |
| | 622.2 | $A_{1g}$ (Mn) | 8.7 |
| | 389 | $E_g$ (Ni) | 5.9 |
| | 451.5 | $E_g$ (Co) | 13.4 |
| | 502.2 | $E_g$ (Mn) | 27.2 |
| AlO-3 | 547.7 | $A_{1g}$ (Ni) | 29.0 |
| | 589 | $A_{1g}$ (Co) | 14.7 |
| | 626.0 | $A_{1g}$ (Mn) | 9.8 |

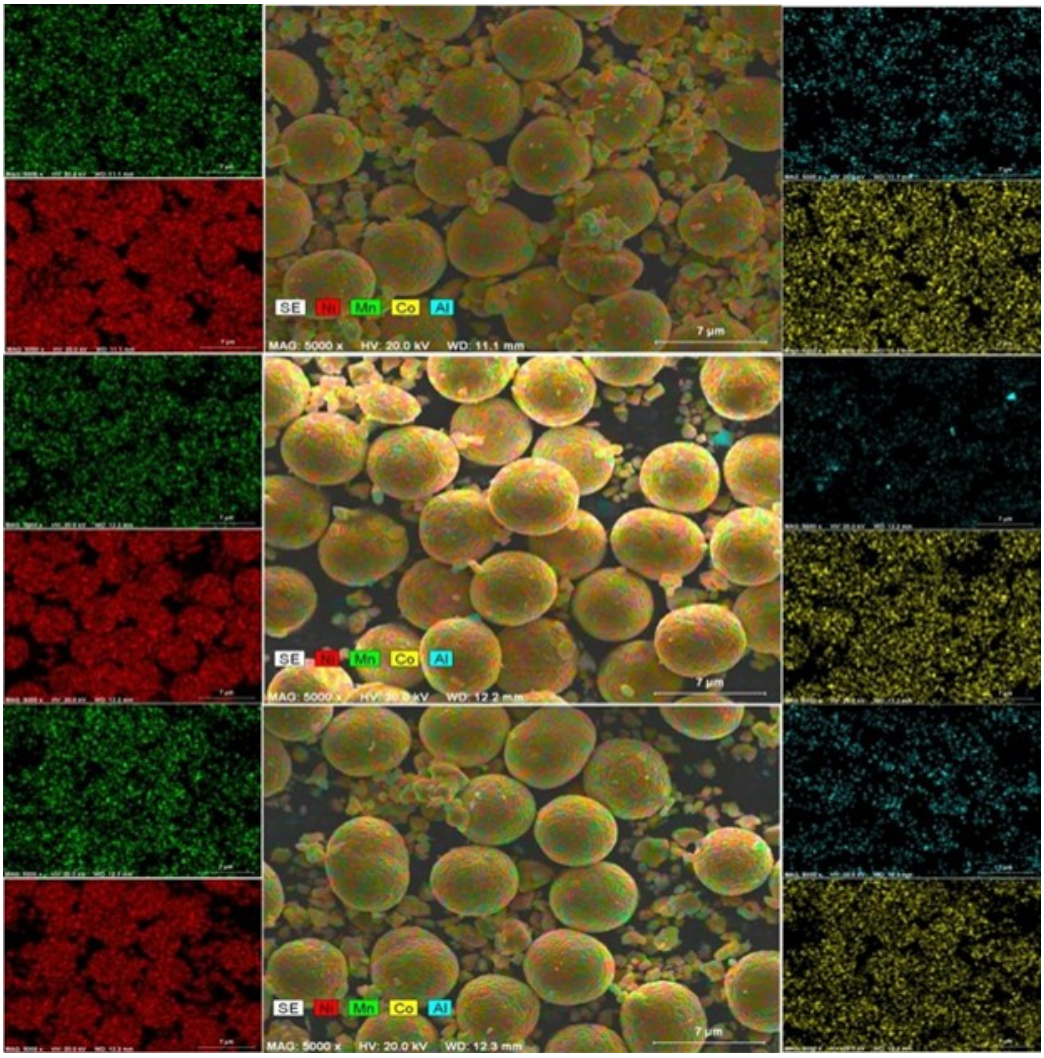


**Fig. S3** SEM-EDX elemental mapping of AlO-1, AlO-2 and AlO-3 powders, showing the spatial distribution of Ni, Mn, Co, and Al on the particle surfaces.

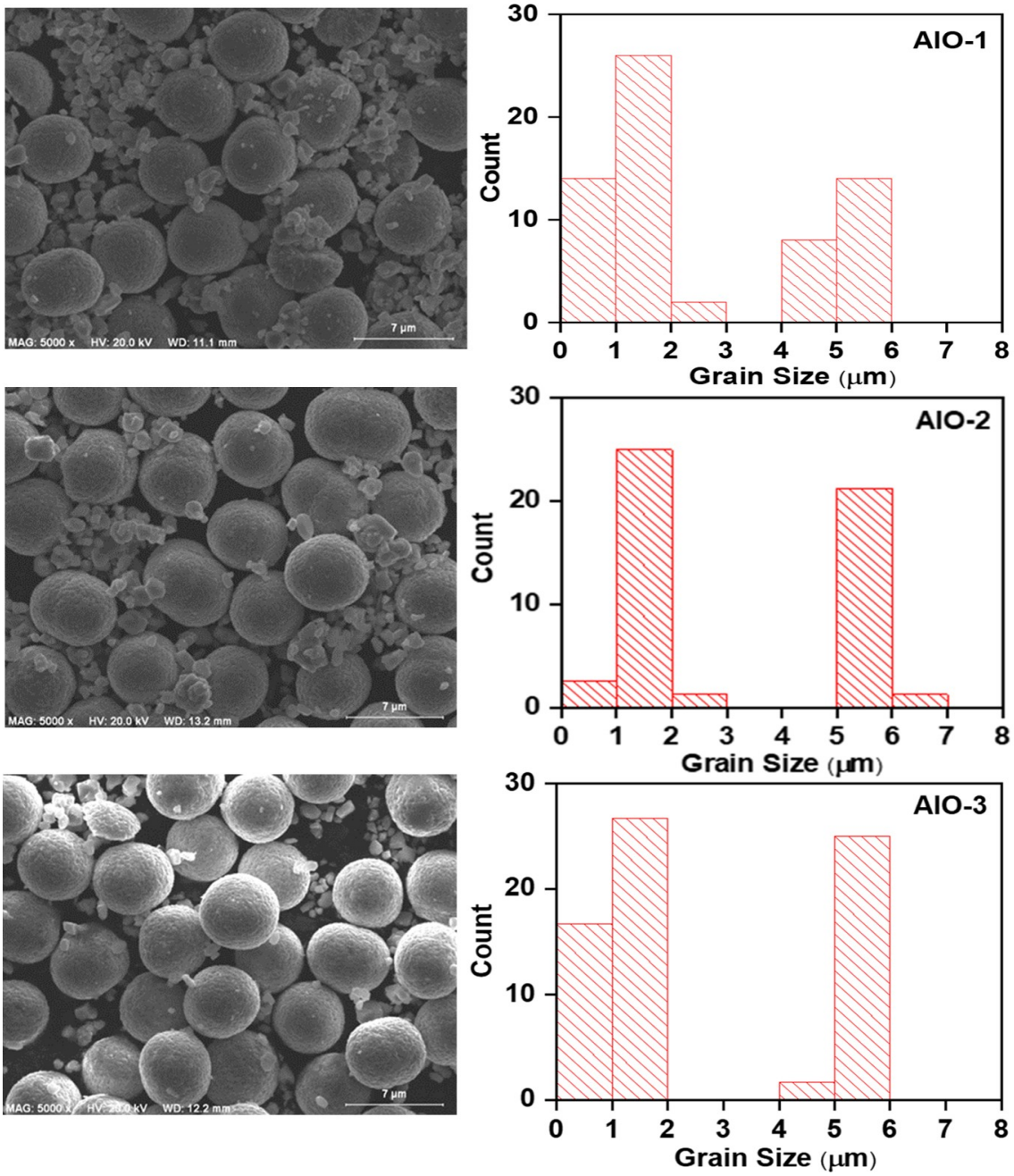


**Fig. S4** Grain sizes of the coated NMC811 samples obtained from SEM images.

**Table S5.** Grain-size values of the coated NMC811 samples.

| Sample ID | Grain size (μm) | Grain size (μm) |
|---|---|---|
| Al01 | 5.15±0.27 | 1.25±0.5 |
| Al02 | 5.29±0.26 | 1.26±0.4 |
| Al03 | 5.50±0.35 | 1.42±0.3 |

**Table S6.** ICP-MS results for pristine NMC811 and $Al_2O_3$-coated NMC811 (AlO-3) powders, with elemental concentrations converted from ppb to atomic ratios.

| Sample ID | Li% | Ni% | Mn% | Co% | Al% |
|---|---|---|---|---|---|
| NMC811 | 50.51 | 41.04 | 2.81 | 5.64 | 0 |
| NMC811@ AlO-3 | 49.35 | 41.74 | 2.83 | 5.74 | 0.34 |

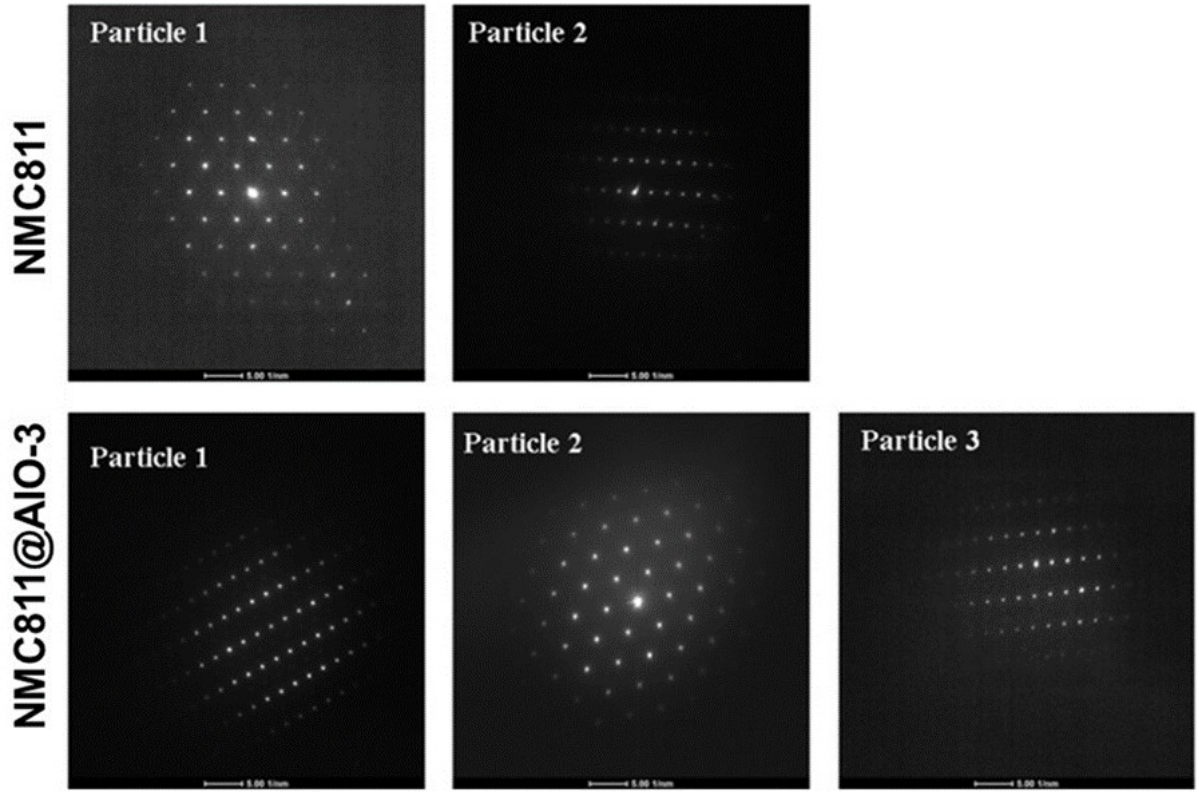


**Fig. S5** SAED patterns of pristine and AlO-3 powders, illustrating the preservation of the layered crystal structure after surface modification.

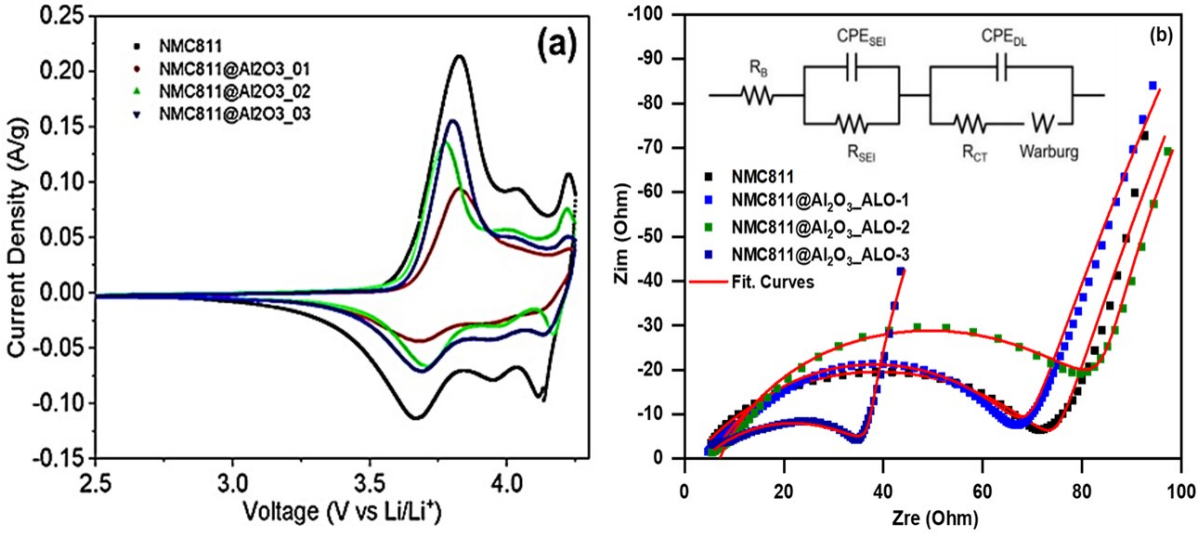


**Fig. S6** (a) and (b) CV and EIS graphs of pristine and NMC811@AlO-3 powders.

**Table S7.** EIS model fitting results for half-cell configurations of pristine and NMC811@$Al_2O_3$ electrodes.

| Parameter | NMC811 | AlO-1 | AlO-2 | AlO-3 |
|---|---|---|---|---|
| $R_b$ | 1.79 | 5.46 | 7.06 | 4.00 |
| $R_{SEI}$ | 73.7 | 64.1 | 80.9 | 35.0 |
| $Q_{ySEI} \times 10^{-5}$ | 0.293 | 3.01 | 4.22 | 15.9 |
| $Q_{aSEI}$ | 0.620 | 0.738 | 0.773 | 0.544 |
| $R_{ct}$ | 13.7 | 35.0 | 30.0 | 23.1 |
| W $\times 10^{-3}$ | 1.01 | 1.11 | 1.23 | 1.61 |
| $Q_{yDL} \times 10^{-3}$ | 2.79 | 2.05 | 0.464 | 0.840 |
| $Q_{aDL}$ | 0.878 | 0.889E | 1.08 | 1.05 |

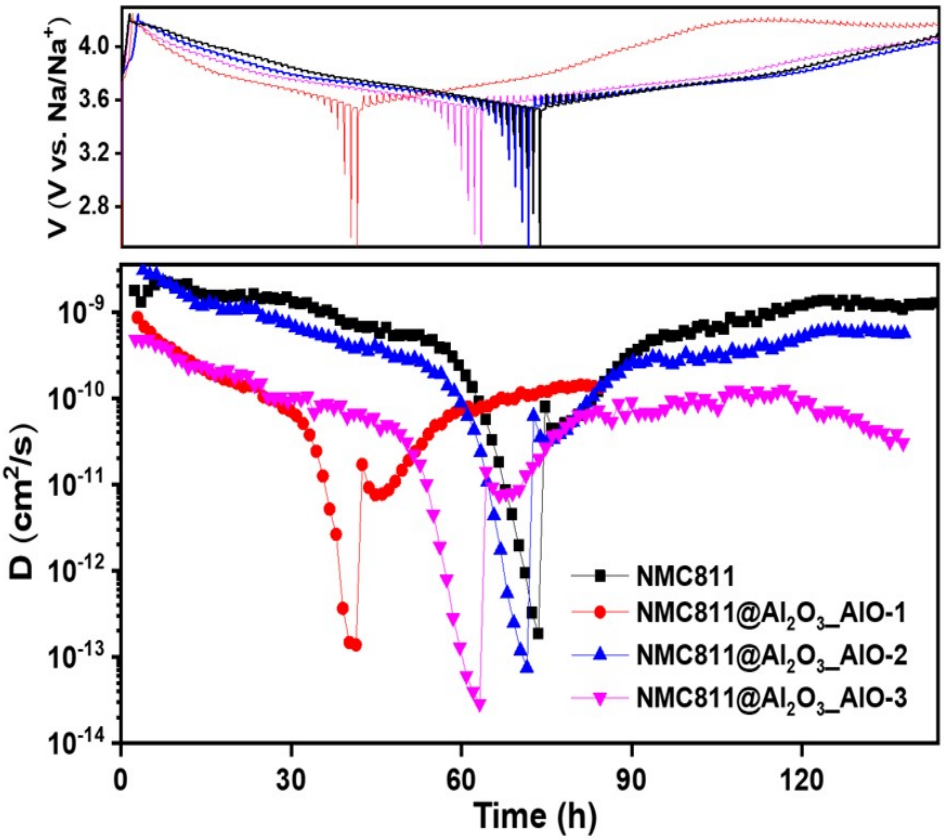


**Fig. S7** Voltage-Time and *D*-time graphs of pristine and NMC811@AlO-3 for GITT measurements.

**Table S8.** Galvanostatic performance analyss of NMC811, $Al_2O_3$-coated NMC811, and graphitic anode electrodes for half cell configuration, along with some previous studies.

| Sample ID | Cur. Density | 1st Cap. (mAh/g) | 25th Cap. (mAh/g) | 50th Cap. (mAh/g) | 100th Cap. (mAh/g) | Capacity Ret. $C_{100}/C_1 \times 100$) | Ref. |
|---|---|---|---|---|---|---|---|
| NMC811 | **C/2** | 181.8 | 167.3 | 156.3 | 136.3 | 74.97 | |
| AlO-1 | | 129.1 | 100.4 | 86.1 | 63.7 | 49.35 | |
| AlO-2 | | 149.5 | 139.2 | 133.7 | 124.3 | 83.14 | |
| AlO-3 | | 159.4 | 148.4 | 144.2 | 134.4 | 84.32 | This |
| Graphite | **30 mA/g** | 351.2 | 307 | 303 | 291 | 82.9 | work |
| Graphene | | 1084 | 830 | 817 | 760 | 70.1 | |
| GO | | 1157 | 703 | 628 | 651 | 56.3 | |

**Previous studies**

| Sample ID | Potential (V vs. $Li^+/Li$) | Capacity | Capacity retention | Ref. |
|---|---|---|---|---|
| $Li_2O$–$B_2O_3$–LiBr@NCM811 | 2.75–4.3V | ~163.5 at 5 C (1 C = 180 mAh/g) | 88.9% (1 C, 200 cycles) | [1] |
| LTO@NCM811 | 0.5–3.0V | 183 mAh/g at 0.5 C | 94.0% (0.5 C, 100 cycles) | [2] |
| PUDMS-NMC811 | 2.8-4.5V | 167 mAh/g at 0.5 C | 80.2% (0.5 C, 200 cycles) | [3] |
| LZC-NMC811 | 2.5-4.5V | 190.8 mAh/g at 0.1 C | 91.0% (0.1 C, 50 cycles) | [4] |

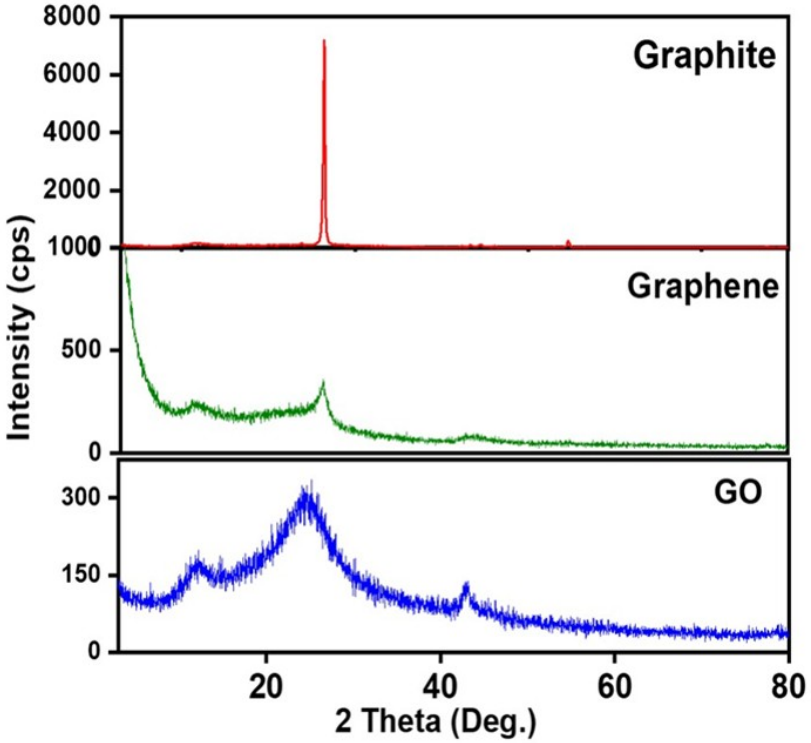


**Fig. S8** XRD patterns of the graphite, graphene and GO powders.

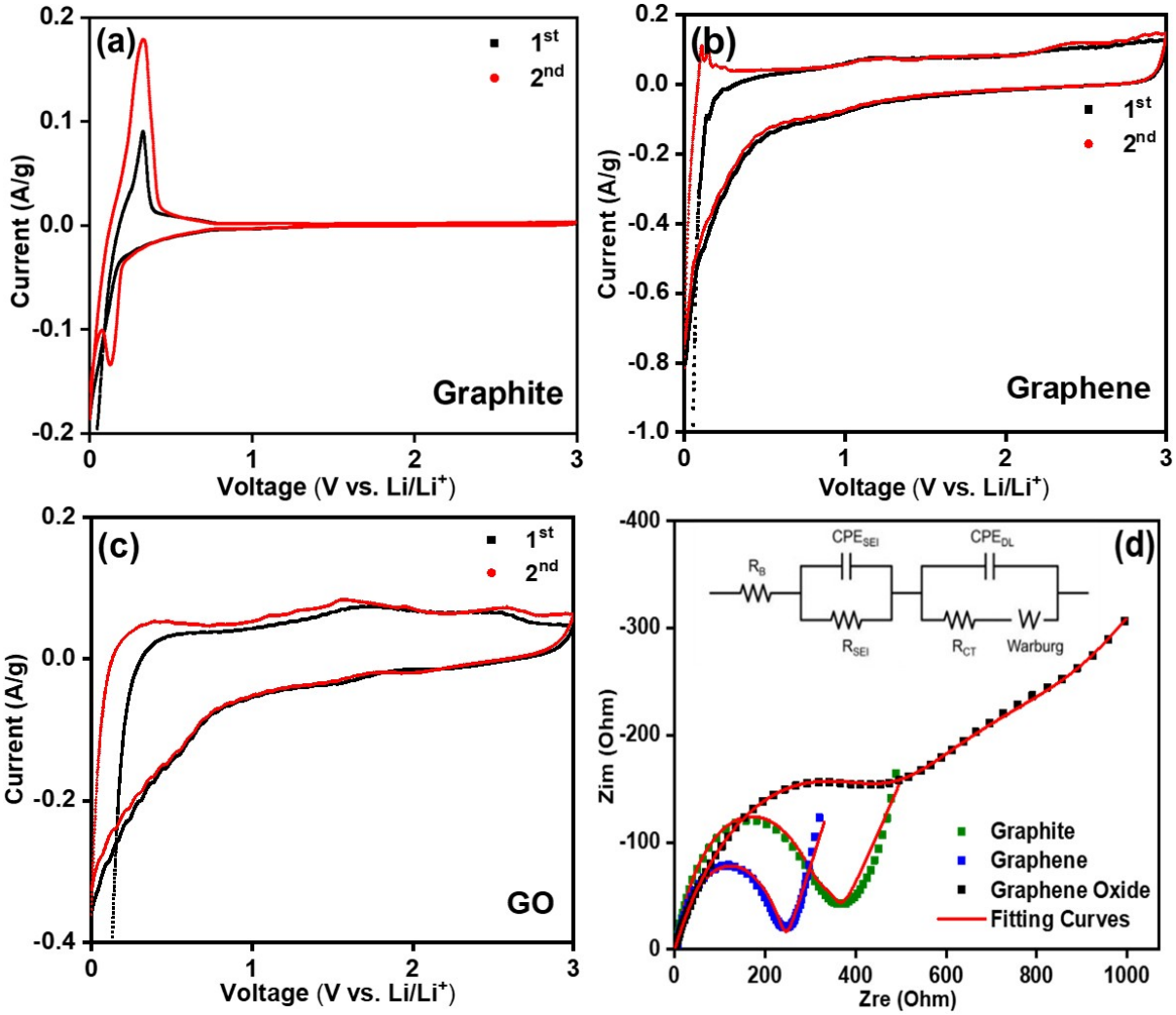


**Fig. S9** CV profiles of (a) graphite. (b) graphene, (c) GO anodes, and (d) EIS analysis of the anode electrodes. The inset in Fig. S7d presents the equivalent circuit model (QCM) employed for data interpretation.

**Table S9.** EIS model fitting results for half-cell configurations of graphitic anode electrodes.

| Parameter | Graphite | Graphene | GO |
|---|---|---|---|
| $R_b$ | 3.60 | 1.76 | 2.22 |
| $R_{SEI}$ | 15.4 | 241 | 159 |
| $Q_{y1} \times 10^{-5}$ | 17.6 | 0.907 | 1.98 |
| $Q_{a1}$ | 1.22 | 0.727 | 0.606 |
| $R_{ct}$ | 325 | 1510 | 1310 |
| W $\times 10^{-3}$ | 3.98 | 0.155 | 1.23 |
| $Q_{y2} \times 10^{-4}$ | 0.053 | 88.1 | 2.47 |
| $Q_{a2}$ | 0.820 | 0.598 | 0.748 |

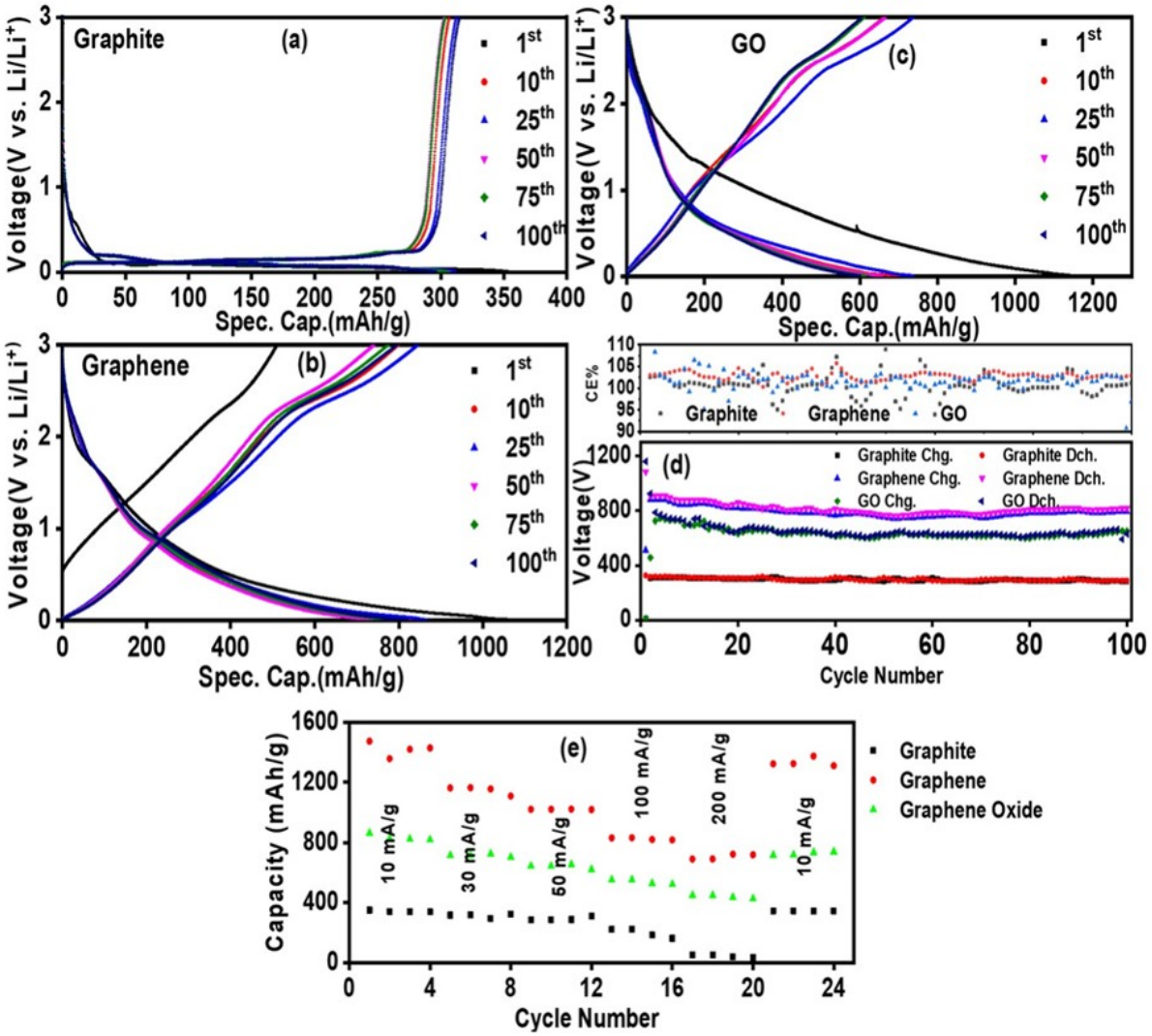


**Fig. S10** Capacity-voltage graphs of half cells (a) graphite, (b) graphene, (c) GO half cells, and (d) capacity-cycle number at constant 30mA/g-rate with coulombic efficiency (CE%), and (e) Different C-rate graphs of graphitic anode electrodes.

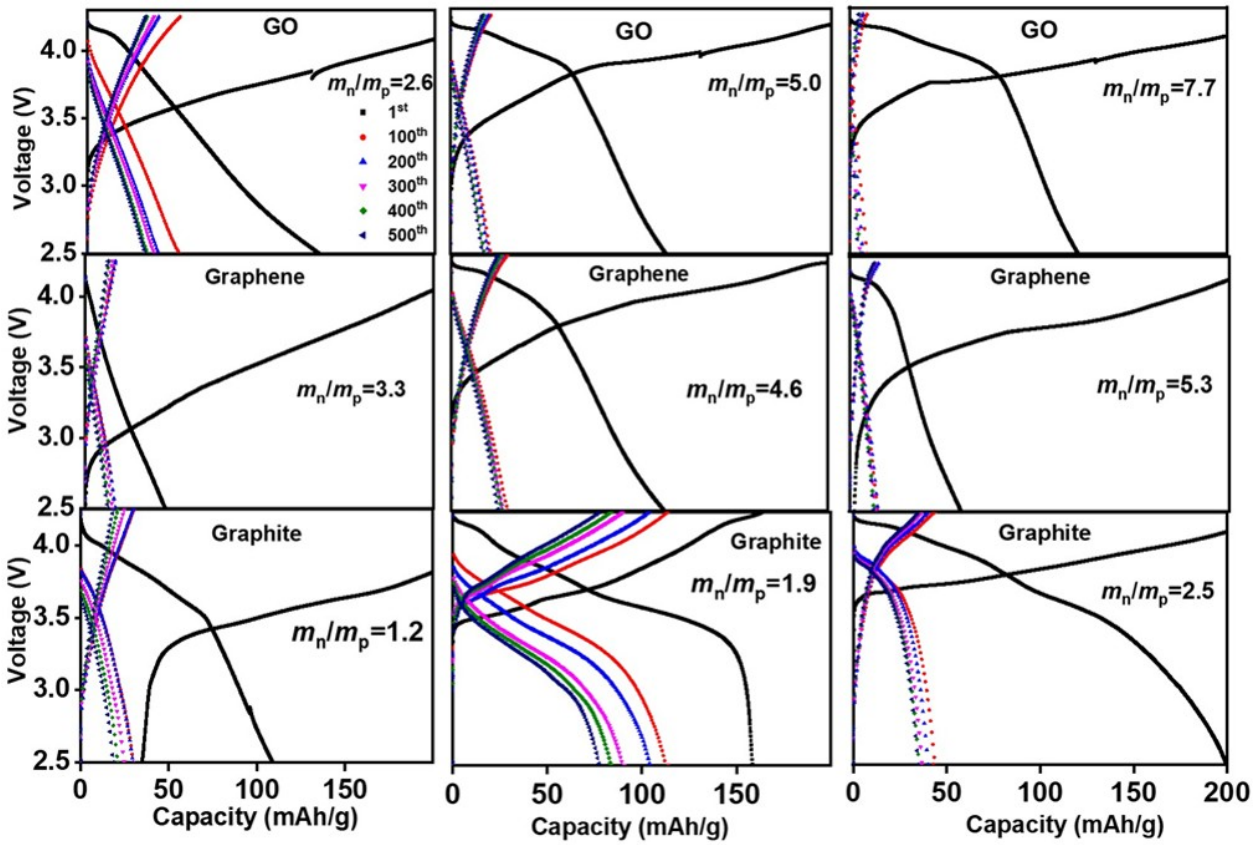


**Fig. S11** Voltage-capacity graphs of NMC811 cathode and graphite, graphene and GO anodes with direct assembling of the cells using different n/p ratio.

**Table S10.** The full-cell parameters and electrode properties with different n/p ratio of the battery cells.

| **Cathode** | | **Anode** | **Theo. Cap.** | **Exp. Cap.** | **Theo. $q_n/q_p$** | **Exp. $q_n/q_p$** | **Ref.** |
|---|---|---|---|---|---|---|---|
| | NMC-811 | Graphite | 372 | 350 | 1.86 | 1.839 | |
| **Theo. Cap.** | 200 | Graphene | 744 | 820 | 3.721 | 4.309 | [5] |
| **Exp. Cap.** | 190.3 | GO | 910 | 1427 | 4.55 | 7.499 | |

| **Cathode** | **Anode** | **$m_n/m_p$** | **Theo. n/p** | **Exp. n/p** | **1st Dch. cap.** | **CE%** |
|---|---|---|---|---|---|---|
| NMC811 | Graphite | 1.2 | 1.52 | 1.50 | 109.01 | 24.77 |
| | Graphite | 1.9 | 0.98 | 0.97 | 158.92 | 83.32 |
| | Graphite | 2.5 | 0.56 | 0.56 | 190.49 | 81.33 |
| | Graphene | 3.3 | 1.13 | 1.31 | 46.22 | 20.38 |
| | Graphene | 4.6 | 0.80 | 0.93 | 113.14 | 52.01 |
| | Graphene | 5.3 | 0.70 | 0.81 | 58.90 | 25.67 |
| | GO | 2.6 | 1.74 | 2.87 | 133.39 | 53.70 |
| | GO | 5.0 | 0.91 | 1.49 | 113.00 | 49.61 |
| | GO | 7.7 | 0.59 | 0.98 | 121.02 | 45.63 |

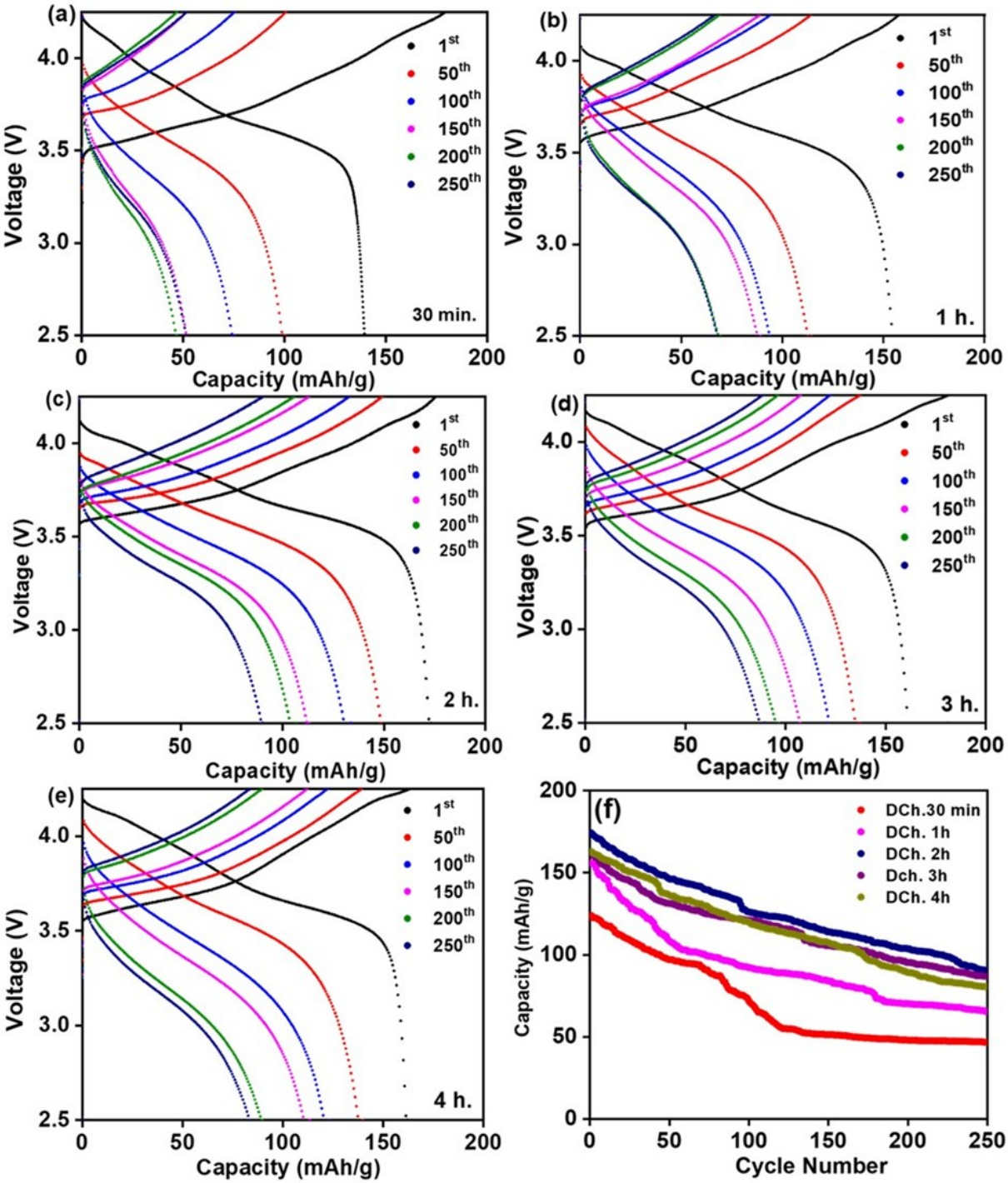


**Fig. S12** Voltage-Capacity graphs of NMC811/graphite full cell with (a) 30 min, (b) 1h, (c) 2h, (d) 3h, (e) 4h pre-lithiation time, and (f) capacity-cycle number graphs of the cells at C/2-rate.

**Table S11.** Optimization of pre-lithiation full cell parameters using NMC811 cathodes/ graphitic anode electrodes.

| Pre-lithation Time | Parameters | Graphite | Graphene | GO |
|---|---|---|---|---|
| 30 min. | OCV (V) | 1.89 | 2.7 | 2.11 |
| | 1. DCh. Cap. (mAh/g) at C/10 | 131.2 | 126.3 | 131.2 |
| | 1st cycle CE % | 59.4 | 78.7 | 55.8 |
| | $m_n/m_p$ | 1.6 | 1.1 | 1.3 |
| | 1. DCh. Cap. (mAh/g) at C/2 | 138.9 | 120.7 | 120.3 |
| | Capacity retention after 250 cycles at C/2 (%) | 33.3 | 56.4 | 56.2 |
| 1 h | OCV (V) | 1.91 | 2.7 | 1.67 |
| | 1. DCh. Cap. (mAh/g) at C/10 | 171.4 | 144.6 | 141.89 |
| | 1st cycle CE % | 61.7 | 69.8 | 3 |
| | $m_n/m_p$ | 1.8 | 1.8 | 2.3 |
| | 1. DCh. Cap. (mAh/g) at C/2 | 154.2 | 138.9 | 138.8 |
| | Capacity retention after 250 cycles at C/2 (%) | 43.6 | 43.9 | 75.9 |
| 2 h | OCV (V) | 2.75 | 2.12 | 2.4 |
| | 1. DCh. Cap. (mAh/g) at C/10 | 177.4 | 154.4 | 156.3 |
| | 1st cycle CE % | 48 | 78.4 | 67.8 |
| | $m_n/m_p$ | 2.1 | 1.7 | 1.3 |
| | 1. DCh. Cap. (mAh/g) at C/2 | 172.1 | 136.8 | 155.9 |
| | Capacity retention after 250 cycles at C/2 (%) | 51.6 | 63.1 | 67.0 |
| 3 h | OCV (V) | 2.66 | 2.74 | 2.24 |
| | 1. DCh. Cap. (mAh/g) at C/10 | 177.4 | 168.9 | 183.1 |
| | 1st cycle CE % | 68.2 | 68.0 | 82.4 |
| | $m_n/m_p$ | 1.5 | 1.1 | 1.36 |
| | 1. DCh. Cap. (mAh/g) at C/2 | 160.1 | 162.5 | 175.2 |
| | Capacity retention after 250 cycles at C/2 (%) | 54.2 | 49.5 | 74.3 |
| 4h | OCV (V) | 2.68 | 2.8 | 1.77 |
| | 1. DCh. Cap. (mAh/g) at C/10 | 184.3 | 150.5 | 170.6 |
| | 1st cycle CE % | 78.9 | 80.2 | 72.7 |
| | $m_n/m_p$ | 2 | 1.1 | 2 |
| | 1. DCh. Cap. (mAh/g) at C/2 | 162.1 | 139.7 | 157.5 |
| | Capacity retention after 250 cycles at C/2 (%) | 51.4 | 61.2 | 71.2 |

*The cathode masses ranged from 1.5–2.6 mg, and the anode masses from 2.1–4.9 mg on 1.5 cm diameter current collectors.

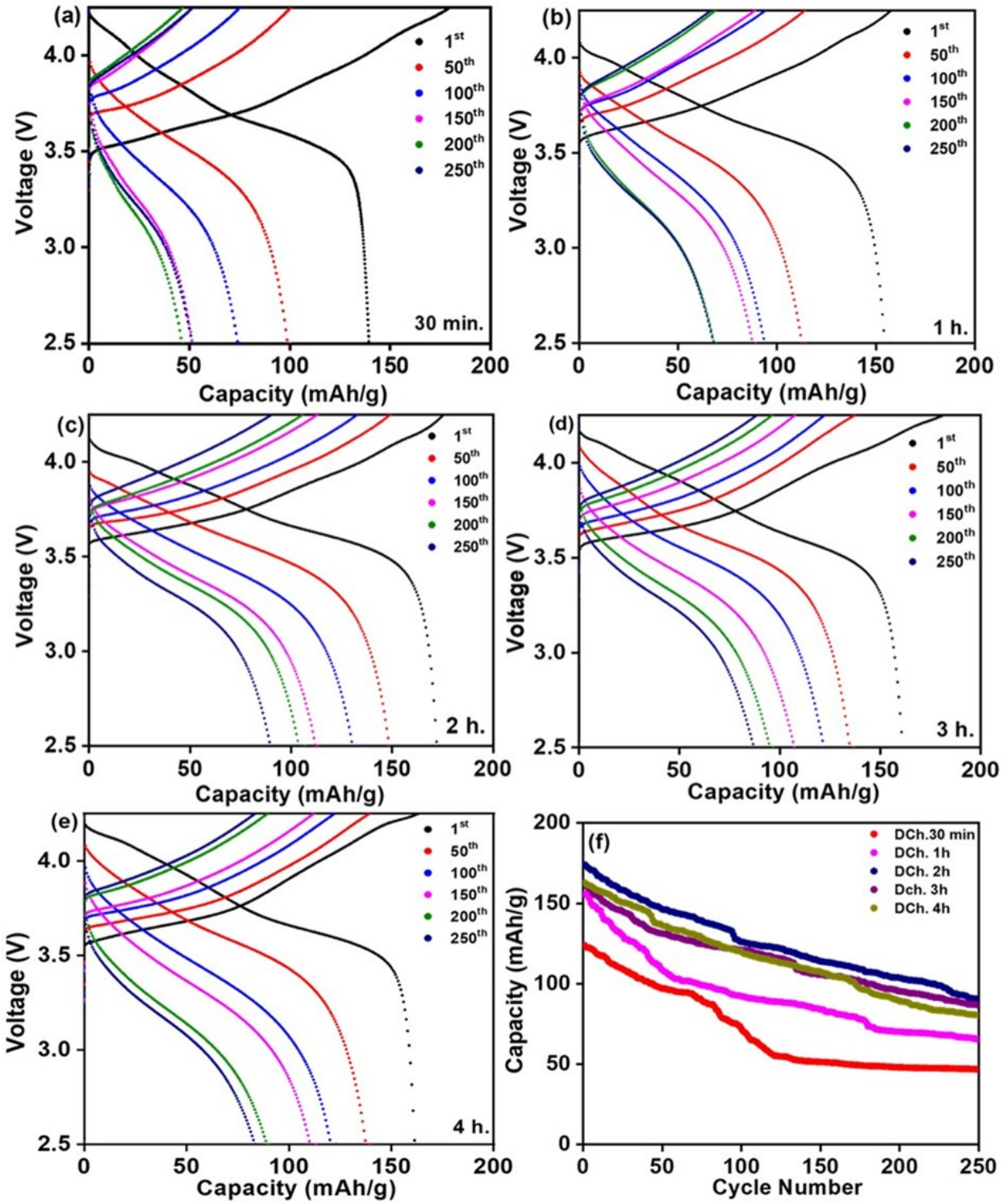


**Fig.S13** Voltage-Capacity graphs of NMC811/graphene full cell with (a) 30 min, (b) 1h, (c) 2h, (d) 3h, (e) 4h pre-lithiation time, and (f) capacity-cycle number graphs of the cells at C/2-rate.

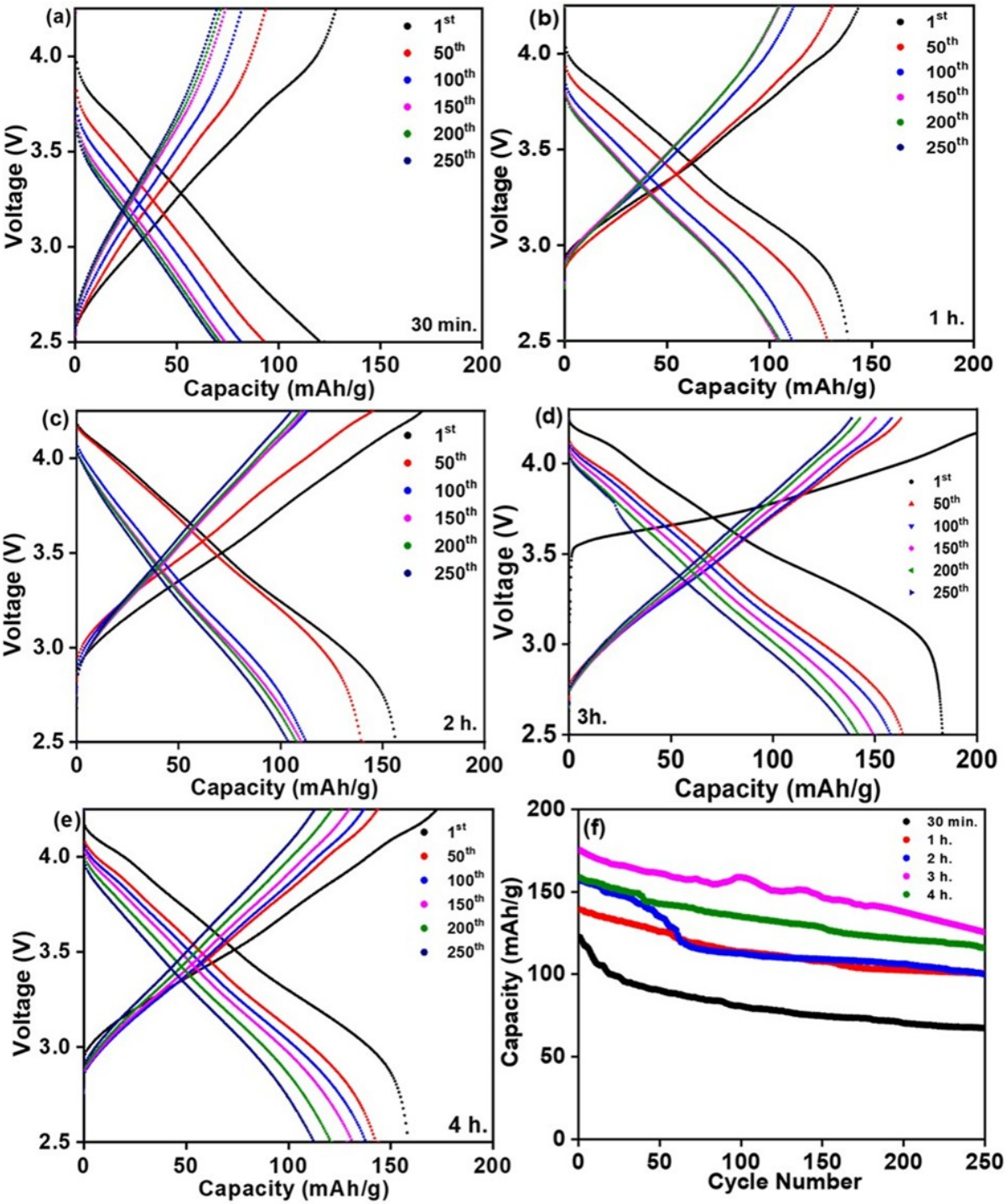


**Fig. S14** Voltage-Capacity graphs of NMC811/GO full cell with (a) 30 min, (b) 1h, (c) 2h, (d) 3h, (e) 4h pre-lithiation time, and (f) capacity-cycle number graphs of the cells at C/2-rate.

**Table S12.** EIS fitting parameters of NMC811@ AlO-3/graphitic anode full cells at optimized pre-lithiation times.

| Parameter | NMC811@ AlO-3/ Graphite | NMC811@ AlO-3/ Graphite | NMC811@ AlO-3/ Graphite |
|---|---|---|---|
| $R_B$ | 3.65 | 2.81 | 2.91 |
| $Q_{y1}$ ×$10^{-3}$ | 1.44 | 1.49 | 1.61 |
| $Q_{a1}$ | 0.879 | 0.876 | 0.959 |
| $R1$ | 453 | 825 | 1030 |
| $Q_{y2}$×$10^{-5}$ | 0.889 | 1.19 | 3.80 |
| $Q_{a2}$ | 0.894 | 0.858 | 0.742 |
| $R_2$ | 19.6 | 16.7 | 6.09 |
| $Q_{y3}$×$10^{-3}$ | 9.20 | 2.42 | 70.4 |
| $Q_{a3}$ | 0.465 | 0.748 | 0.340 |
| $R_3$ | 15.9 | 23.8 | 26.1 |

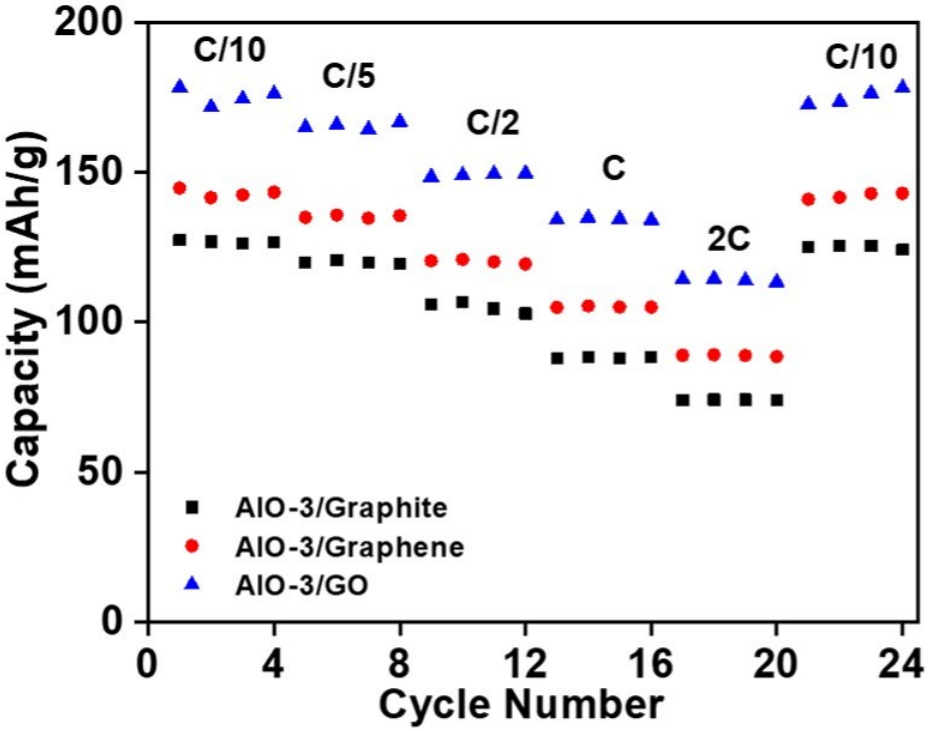


**Fig. S15** C-rate performance of NMC811@AlO-3 cathode full cells employing pre-lithiated graphite, graphene, and graphene oxide as anodes.

## References


[1] T. Wang, M. Yuan, Y. Liu, H. Liu, S. Xie, J. Liu, J. Yan, Improving the electrochemical performance of Ni-rich cathode materials using a fast ion conductor coating of $Li_2O$–$B_2O_3$–LiBr, *Ceram. Int*., **48** (2022) 3397–3403.

[2] M. Han, J. Duan, Z. Wang, W. Wu, W. Luo, Evaluation of Cathode Electrodes in Lithium-Ion Battery: Pitfalls and the Befitting Counter Electrode, *Small*, 2023, **19**, 2208018.

[3] X. Liu, X. Xu, J. Li, M. Yang, Y. Xu, J. Zhu, J. Chen, Y.J. Cheng, Y. Gao, Y. Xia, Tiny, yet sufficient: 25% of capacity retention increase with NCM811 cathode realized by 1.5% of block copolymer modification, *J. Energy Storage*, 2024, **93**, 112256.

[4] H. J. Jeon, R. Rajagopal, J. Park, S. Kang, K. S. Ryu, Surface modification of Li ($Ni_{0.8}Co_{0.1}Mn_{0.}$) $O_2$ with $Li_2ZrCl_6$ halide solid electrolyte for all-solid-state batteries. *J. Ind. Eng. Chem*., 2025, **149**, 461–468.

[5] D. Kornilov, T. R. Penki, A. Cheglakov, D. Aurbach, Li/graphene oxide primary battery system and mechanism, *Battery Energy*, 2022, **1**, 20210002.